

High-tolerance antiblockade SWAP gates using optimal pulse drivings

Wan-Xia Li¹, Jin-Lei Wu², Shi-Lei Su², and Jing Qian¹

¹*State Key Laboratory of Precision Spectroscopy,
Department of Physics, School of Physics and Electronic Science,
East China Normal University, Shanghai, 200062, China and*
²*School of Physics, Zhengzhou University, Zhengzhou 450001, China**

Position error is treated as the leading obstacle that prevents Rydberg antiblockade gates from being experimentally realizable, because of the inevitable fluctuations in the relative motion between two atoms invalidating the antiblockade condition. In this work we report progress towards a high-tolerance antiblockade-based Rydberg SWAP gate enabled by the use of modified antiblockade condition combined with carefully-optimized laser pulses. Depending on the optimization of diverse pulse shapes our protocol shows that the time-spent in the double Rydberg state can be shortened by a factor of $> 70\%$, which significantly reduces the position error. Moreover, we benchmark the robustness of the gate via taking account of the technical noises, such as the Doppler dephasing due to atomic thermal motion, the fluctuations in laser intensity and laser phase and the intensity inhomogeneity. As compared with other existing antiblockade-gate schemes the predicted gate fidelity is able to maintain at above 0.91 after a very conservative estimation of various experimental imperfections, especially considered for realistic interaction deviation of $\delta V/V \approx 5.92\%$ at $T \sim 20 \mu\text{K}$. Our work paves the way to the experimental demonstration of Rydberg antiblockade gates in the near future.

I. INTRODUCTION

Implementation of Rydberg antiblockade gates is one of the current mainstream protocols towards fast and robust neutral-atom quantum computation [1–7], as the traditional Rydberg antiblockade regime with enhanced dissipative dynamics can lead to the preparation of high-fidelity steady entanglement in versatile systems [8–17]. Beyond applications in quantum entanglement, constructing a quantum logic gate via antiblockade mechanism [18–20] is more straightforward because the simultaneous multi-atom excitation establishes an effective model which exactly avoids the occupancy of lossy singly-excited Rydberg states [21]. Despite these significant advances, however, owing to the leading participation of multi-atom excited states, such antiblockade gates are found to be extremely sensitive to the relative position fluctuations between two atoms [22–25] as well as to the atomic decays [26–28], which inherently forbids its experimental validation.

Based on antiblockade mechanism, some prior studies of e.g. control-phase gates [29], presented the gate infidelity far larger than 0.15 for a interaction deviation of $\delta V/V \approx 5.0\%$. More recently, Wu *et.al.* [30] demonstrated the two-atom SWAP gates with a infidelity of ~ 0.03 when the position deviation in the interatomic distance is only ~ 3.0 nm, necessarily for using a deep cooling of ground-state atomic qubits [31–33] or sufficiently deep traps [34]. Therefore, although the antiblockade mechanism can lead to high-fidelity Rydberg gates in theory, to implement them in experiment remains untouchable yet. A practical position-error-tolerant scheme is urgently needed.

In this work we present a practical scheme to realize the antiblockade SWAP gates with greatly improved tolerance, especially, to the fluctuations of interatomic interaction. We perform optimizations to three different laser pulse shapes towards the target of minimizing time-spent in the double Rydberg state [35], so as to decrease the sensitivity of gate respect to the interatomic distance deviation. It is observable that, accompanied by a *modified antiblockade* condition $V = \Delta_1 + \Delta_2 + q$ (in contrast to the *perfect antiblockade* regime where $q = 0$) which contains an adjustable factor q to loosen the antiblockade constraint and hence to affect the multi-atom excitation probability, the occupancy of double Rydberg state can be greatly suppressed under diversely optimized pulses [36]. The ideal two-qubit SWAP gates in the absence of any position deviations, have an average fidelity reaching $\mathcal{F} \sim 0.9997$. Even taking account of other technical imperfections a more conservative estimation arises $\mathcal{F} \geq 0.9142$ for a typical $1.0\text{-}\mu\text{s}$ gate time, which is mainly limited by the position error ~ 0.075 considered for an atomic temperature of $T \sim 20 \mu\text{K}$ (equivalently $\delta V/V \approx 5.92\%$). An extensive study in the appendix B shows that, a faster ($\sim 0.1 \mu\text{s}$) antiblockade SWAP with high-tolerance is feasible at the expense of stronger laser Rabi frequencies.

Our implementation building on the earlier proposal of antiblockade gates [30], additionally adopts optimal pulse drivings, which, not only avoids the combination of a series of elementary gates [37] and realizes the nontrivial SWAP gate within one-step implementation; but also greatly improves the antiblockade-gate robustness against intrinsic position fluctuations between two trapped atoms. The SWAP gate is important with extensive applications in e.g., quantum entanglement swapping [38–40] and quantum repeater [41–43]. As compared to other existing proposals the parameters we set to real-

* jqian1982@gmail.com

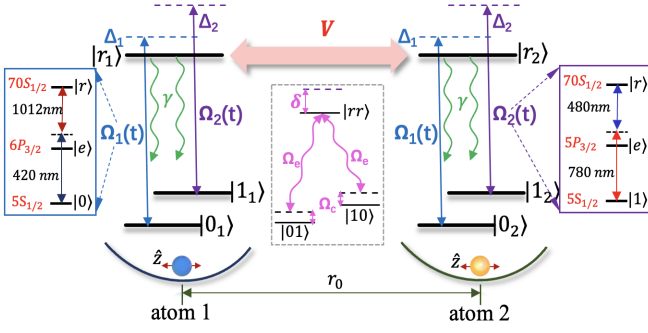


FIG. 1. Level structure of a two-qubit Rydberg SWAP gate based on *modified antiblockade* mechanism. The central box inset shows an effective swapping model formed by an off-resonance Raman-like transition on two targeted states $|01\rangle$ and $|10\rangle$. The qubits are defined as hyperfine clock qubits encoded in $|0_{1,2}\rangle = |5S_{1/2}, F=1, M_F=0\rangle$ and $|1_{1,2}\rangle = |5S_{1/2}, F=2, M_F=0\rangle$. $|r_{1,2}\rangle = |70S_{1/2}\rangle$ is a Rydberg state considered for a rubidium-87 atomic experiment [44]. The van der Waals dispersion coefficient for $|70S_{1/2}; 70S_{1/2}\rangle$ is $C_6/2\pi = 862.69 \text{ GHz}\cdot\mu\text{m}^6$ [45], leading to the non-fluctuated Rydberg-Rydberg interaction $V/2\pi \approx 70.49 \text{ MHz}$ at a fixed distance $r_0 = 4.8 \mu\text{m}$. The rate of spontaneous emission is $\gamma = 2\pi/\tau$ with $\tau (\approx 400 \mu\text{s})$ being the lifetime of Rydberg states $|r_{1,2}\rangle$. See text for more details.

ize the gate, are all extracted from precise-optimization which can provide an opportunity to decrease the leading contribution i.e., the position error that mainly restricts the antiblockade gate fidelity.

II. THEORETICAL STRATEGY

In this paper we propose a two-qubit SWAP gate with high position-error tolerance based on the *modified antiblockade* condition. As illustrated in Fig.1, two identical neutral atoms individually trapped in two optical tweezers, have hyperfine ground states $|0\rangle$, $|1\rangle$ and Rydberg state $|r\rangle$. The subscripts $1,2$ have been omitted. They interact with an energy V when both atoms are excited to $|r\rangle$. During the laser-based operation we consider the time-dependent pulses $\Omega_1(t)$ (detuning Δ_1) and $\Omega_2(t)$ (detuning Δ_2) coupling $|0\rangle \rightarrow |r\rangle$ and $|1\rangle \rightarrow |r\rangle$, are two-photon transitions [46] via two different low-lying p states. State $|r\rangle$ decays to $|0\rangle$, $|1\rangle$ with rate γ and equal branching ratios.

In the interaction picture the full Hamiltonian can be described by ($\hbar = 1$)

$$\hat{H} = \hat{H}_1 \otimes \hat{I}_2 + \hat{I}_1 \otimes \hat{H}_2 + \hat{V}_{rr} \quad (1)$$

where

$$\hat{H}_j = \Omega_1 e^{-i\Delta_1 t} |0_j\rangle \langle r_j| + \Omega_2 e^{-i\Delta_2 t} |1_j\rangle \langle r_j| + \text{H.c.} \quad (2)$$

and

$$\hat{V}_{rr} = V |rr\rangle \langle rr| \quad (3)$$

with $j \in (1, 2)$ and $V = \Delta_1 + \Delta_2 + q$ being the Rydberg interaction strength. Here, q is a nontrivial factor and $q = 0$ means the *perfect antiblockade* condition enabling a facilitation of the double Rydberg state $|rr\rangle$ [47, 48]. But, when $q \neq 0$ known as the *modified antiblockade* condition it could reduce the population on $|rr\rangle$ by canceling some unwanted ac Stark shifts [49]. By using the second-order perturbation theory for the full Hamiltonian (1) combined with the condition of large detunings $|\Delta_1| \gg \Omega_1$, $|\Delta_2| \gg \Omega_2$, we can outline the state transfer in the effective swapping model. When the initial state is $|00\rangle$ or $|11\rangle$ the effective Hamiltonian associated becomes

$$\hat{H}_{00,eff} = \frac{2\Omega_1^2}{\Delta_1} |00\rangle \langle 00| \quad (4)$$

$$\hat{H}_{11,eff} = \frac{2\Omega_2^2}{\Delta_2} |11\rangle \langle 11| \quad (5)$$

which are dark to all gate pulses as expected. Whereas if the initially-considered states are $|01\rangle$ or $|10\rangle$ the full Hamiltonian (1) can be reduced into a same effective formula, like

$$\begin{aligned} \hat{H}_{01,eff} = & \Omega_e (|rr\rangle \langle 01| + |rr\rangle \langle 10|) + \text{H.c.} \\ & + \Omega_c (|01\rangle \langle 01| + |10\rangle \langle 10|) + \delta |rr\rangle \langle rr| \end{aligned} \quad (6)$$

with

$$\Omega_e = \frac{\Omega_1 \Omega_2}{\Delta_1} + \frac{\Omega_1 \Omega_2}{\Delta_2}, \Omega_c = \frac{\Omega_1^2}{\Delta_1} + \frac{\Omega_2^2}{\Delta_2}, \delta = \frac{2\Omega_2^2}{\Delta_1} + \frac{2\Omega_1^2}{\Delta_2} + q \quad (7)$$

denoting the effective couplings, the ac Stark shift with respect to $|01\rangle$ and $|10\rangle$ and the effective detuning to $|rr\rangle$. More details about the derivation of Eqs.(4-6) can be found in appendix A. Here states $|01\rangle$ and $|10\rangle$ exhibit equivalent dynamics in this symmetric setup so $\hat{H}_{01,eff} = \hat{H}_{10,eff}$.

From $\hat{H}_{01,eff}$ we find an effective three-level system for states $|01\rangle$ and $|10\rangle$ which is off-resonantly coupled to $|rr\rangle$, as shown in the central inset of Fig.1. One thus expects the combined action of all quantities Ω_e , Ω_c , δ will achieve a perfect state swapping by obeying $|01\rangle \rightleftharpoons |rr\rangle \rightleftharpoons |10\rangle$. However, the participation of simultaneous Rydberg excitation state $|rr\rangle$ in this process must suffer from a serious position error i.e. mainly caused by the significant deviation of interatomic interaction $\delta V/V$ between individually trapped atoms [50]. Remarkably, here the effective detuning δ contains a factor q which provides a flexible adjustment to the ac Stark shift on state $|rr\rangle$. Although this original ac shift term $\frac{2\Omega_2^2}{\Delta_1} + \frac{2\Omega_1^2}{\Delta_2}$ is time-dependent during the gate pulses; yet applying a nonzero q is able to enlarge the effective detuning and so as to reduce the intermediate-state population [51]. In a practical situation with significant interaction fluctuations, we observe that, with the help of *modified antiblockade* condition our protocol can exhibit a higher tolerance against these deviations which arise from e.g. the thermal motion of atoms in the inhomogeneous coupling field [52] or laser intensity noise [53].

III. GATE IMPLEMENTATION WITH OPTIMAL PULSES

Now we discuss the implementation of the two-qubit SWAP gates under diverse pulse shapes. The numerical optimization of pulse shapes $\Omega_1(t)$, $\Omega_2(t)$ is performed using genetic algorithm for maximizing the gate fidelity as in our prior work [54]. Notice that all deviations arising from technical imperfections are excluded in the optimization, and we will analyze the gate robustness against them in later sections. To fully understand the population dynamics we have numerically solved the two-atom master equation in the Lindblad form [55],

$$\dot{\rho} = -i[\hat{\mathcal{H}}, \rho] + \frac{1}{2} \sum_{j=1}^4 [2\hat{\mathcal{L}}_j \hat{\rho} \hat{\mathcal{L}}_j^\dagger - (\hat{\mathcal{L}}_j^\dagger \hat{\mathcal{L}}_j \hat{\rho} + \hat{\rho} \hat{\mathcal{L}}_j^\dagger \hat{\mathcal{L}}_j)] \quad (8)$$

where the one-atom decay operator $\hat{\mathcal{L}}_j$ expressed in the basis $\{|0\rangle, |1\rangle, |r\rangle\}$ is

$$\hat{\mathcal{L}}_{1(2)} = \sqrt{\frac{\gamma}{2}} |0(1)_1\rangle \langle r_1|, \hat{\mathcal{L}}_{3(4)} = \sqrt{\frac{\gamma}{2}} |0(1)_2\rangle \langle r_2| \quad (9)$$

representing the four spontaneous decay channels. Here we have assumed state $|r_{1(2)}\rangle$ decays to $|0_{1(2)}\rangle$ and $|1_{1(2)}\rangle$ with an equal probability $\gamma/2$. Numerical solutions of Eq.(8) can be directly used to define the average gate fidelity over four input states $\{|00\rangle, |01\rangle, |10\rangle, |11\rangle\}$ as

$$\mathcal{F} = \frac{1}{4} \text{Tr} \sqrt{\sqrt{U} \rho(t = T_g) \sqrt{U}} \quad (10)$$

with U the ideal matrix for the two-qubit SWAP gates and $\rho(t)$ the practical density matrix measured at $t = T_g$ (total gate time). For a specific input state one can simulate the full dynamics of arbitrary intermediate state by obeying the above master equation.

To obtain an antiblockade SWAP gate with high tolerance the leading step is to find out optimal pulse shapes with an appropriate q , which minimizes the time-spent in the Rydberg level, especially in the double Rydberg state $|rr\rangle$. For comparison we demonstrate the gate using different optimized shaped pulses [56]. The time scale T_g for the gate is constrained by the maximal Rabi frequency of the driving lasers that should meet the swapping circles. Here T_g is set to be $1.0 \mu\text{s}$ which restricts the maximal strength of Rabi frequencies to be approximately $2\pi \times 10$ MHz. Also, in order to show the significance of q we seek for optimal pulse parameters individually under two cases: $q = 0$ and $q \neq 0$ which are summarized in Table I. The corresponding full dynamics are comparably displayed in Fig. 2.

First we demonstrate the gate with two optimal isosceles-triangle-shaped pulses via assuming

$$\begin{aligned} \text{Case } i: \Omega_j(t) &= \Omega_j^{\max} \text{ when } t = \frac{T_g}{2} \\ \Omega_j(t) &= 0 \text{ when } t = 0, T_g \end{aligned}$$

TABLE I. Optimal pulse parameters and detunings under three different pulse waveforms for $q = 0$ and $q \neq 0$. Parameters such as Ω_j^{\max} , Ω_{0j} , Ω_{1j} , Ω_{2j} , Δ_1 , q are all in units of $2\pi \times \text{MHz}$, and ω_j is in unit of μs . In any case the antiblockade condition $V = \Delta_1 + \Delta_2 + q$ is always satisfied and $V = 2\pi \times 70.49$ MHz treats as the ideal(non-fluctuated) interaction strength between two atoms at a fixed distance r_0 . The ideal gate fidelity \mathcal{F} calculated at zero temperature is given in the last column. The intrinsic decay error caused by the limited lifetime of Rydberg levels, can be estimated by $1 - \mathcal{F}$.

Case i: Isosceles-triangle pulses				
q	Ω_1^{\max}	Ω_2^{\max}	Δ_1	\mathcal{F}
0	3.769	10.441	26.642	0.9992
4.668	5.513	10.947	23.090	0.9996
Case ii: Gaussian pulses				
q	$(\Omega_1^{\max}, \Omega_2^{\max})$	(ω_1, ω_2)	Δ_1	\mathcal{F}
0	(3.595, 9.219)	(0.279, 0.189)	23.924	0.9993
5.037	(5.114, 8.948)	(0.257, 0.351)	22.110	0.9997
Case iii: Composite pulses				
q	$(\Omega_{01}, \Omega_{11}, \Omega_{21})$	$(\Omega_{02}, \Omega_{12}, \Omega_{22})$	Δ_1	\mathcal{F}
0	(1.033, -1.167, 1.334)	(3.100, -2.662, 2.617)	25.194	0.9992
5.090	(1.774, -1.884, 2.036)	(2.558, -2.624, 2.608)	22.532	0.9997

This triangular pulse involves only one parameter Ω_j^{\max} to be optimized except Δ_1 and q . Through comparing Fig.2(a1-e1) and (a4-e4), we observe that, although the optimal pulse maxima Ω_1^{\max} and Ω_2^{\max} are comparable with each other; yet case (a4-e4) with $q \neq 0$ clearly leads to a larger energy shift $\delta(t)$ (see the green-dashed line in (b4)) which allows a big reduction in the time-spent of the double Rydberg state. We verify this by calculating the duration to be in state $|rr\rangle$ for input $|01\rangle$ and find that in (e1) with $q = 0$, $T_{rr} = \int_0^{T_g} \rho_{rr}(t) dt \approx 0.0926 \mu\text{s}$. While this value is reduced to $0.0248 \mu\text{s}$ in the case of (e4) where $q/2\pi = 4.668$ MHz (optimal). Due to an approximately 73.2% reduction in the time-spent, the intrinsic decay error also obtains a large decrease yielding $\mathcal{F} \approx 0.9996$. We illustrate the validity of the effective Hamiltonian (6) by simulating the effective population dynamics of states $|01\rangle$, $|rr\rangle$ and $|10\rangle$ in (e1) and (e4). A good coincidence between the full and effective models are explicit confirming the accuracy of our perturbation theory [57].

Furthermore after taking account of the convenience of experimental demonstration, we turn to demonstrate the SWAP gate with smoother pulses which contain more

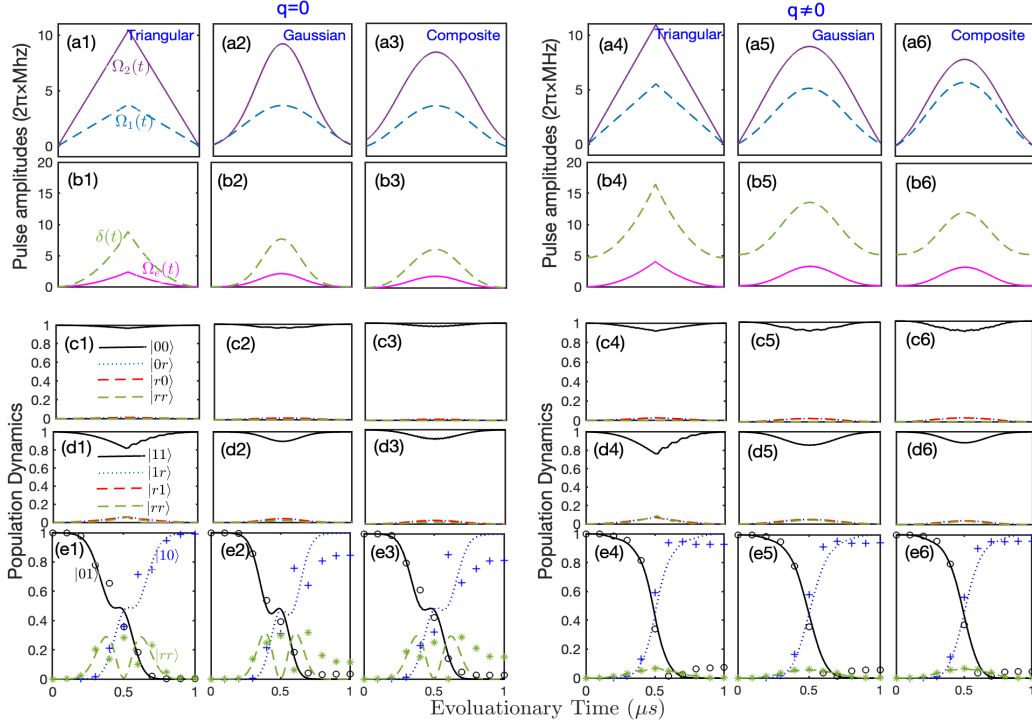


FIG. 2. Realization of two-qubit SWAP gates with different optimal pulse shapes. (a1,a4) Optimal isosceles-triangle waveforms $\Omega_1(t)$, $\Omega_2(t)$ and (b1,b4) optimal effective coupling $\Omega_e(t)$ and effective detuning $\delta(t)$ versus the evolutionary time $t \in [0, 1.0]$ μs . $q = 0$ and $q \neq 0$ stand for the *perfect antiblockade* and *modified antiblockade* cases. The corresponding time-dependent population dynamics based on the original Hamiltonian $\hat{\mathcal{H}}$ with different initial states $\{|00\rangle, |11\rangle, |01\rangle\}$, are respectively displayed in (c1,c4), (d1,d4), (e1,e4). In (e1) and (e4) the population dynamics of states $|01\rangle$, $|10\rangle$, $|rr\rangle$ based on the effective Hamiltonian $\hat{\mathcal{H}}_{01,eff}$ are described by black-circles, blue-crosses and green-stars. Similarly, results with optimal Gaussian and composite pulse shapes are given in (a2-e2,a5-e5) and (a3-e3,a6-e6).

parameters to be optimized [58]. They are

$$\text{Case ii: } \Omega_j(t) = \Omega_j^{\max} \left[\frac{e^{-(t-T_g/2)^2/2\omega_j^2} - e^{-(T_g/2)^2/2\omega_j^2}}{1 - e^{-(T_g/2)^2/2\omega_j^2}} \right]$$

$$\text{Case iii: } \Omega_j(t) = \Omega_{0j} + \Omega_{1j} \cos\left(\frac{2\pi t}{T_g}\right) + \Omega_{2j} \sin\left(\frac{\pi t}{T_g}\right).$$

while keeping Δ_1 and q optimal values. $\Delta_2 = V - \Delta_1 - q$ is always fulfilled. Particularly, in *Case ii* the Gaussian function has been corrected by allowing an exact zero intensity at the start and end of the pulse, which, from an experimental point of view, has a better feasibility [59]. Finally we present the optimal smooth pulses and the population dynamics separately in Fig.2(a2-e2;a5-e5) and (a3-e3;a6-e6). It is observable that, if $q \neq 0$ the time-spent in state $|rr\rangle$ remains at a low level i.e. $T_{rr} \approx (0.0238, 0.0254)$ μs , arising a slightly higher fidelity $\mathcal{F} \approx 0.9997$ than the triangular pulse. Note that, here although the effective state swapping between $|01\rangle$ and $|10\rangle$ also requires the participation of $|rr\rangle$, its influence has been deeply suppressed by applying pulse optimization under the *modified antiblockade* condition. A rough

estimation to the intrinsic Rydberg decay error gives to a small value $1 - \mathcal{F} = (3 \sim 4) \times 10^{-4}$ which is very robust to arbitrary pulse shapes.

So far we have verified that, the participation of antiblockade condition facilitates the simultaneous excitation from the ground state to the double Rydberg state suppressing the influence from intermediate single excitation states, which results in an efficient one-step implementation of Rydberg gates. Nevertheless, the leading obstacle that limits the robustness of such antiblockade gates, becomes its sensitivity in practice to the interaction fluctuations between two atoms on this double Rydberg state. Typically they do depend on “frozen” Rydberg atomic interactions so as to fulfill the antiblockade condition [60, 61]. In the present work by minimizing the time-spent in $|rr\rangle$ together with the merit of small decay errors, the gate tolerance to the interaction fluctuations can be largely improved, promising for a high-fidelity quantum gate with hotter atoms.

IV. POSITION ERROR TOLERANCE

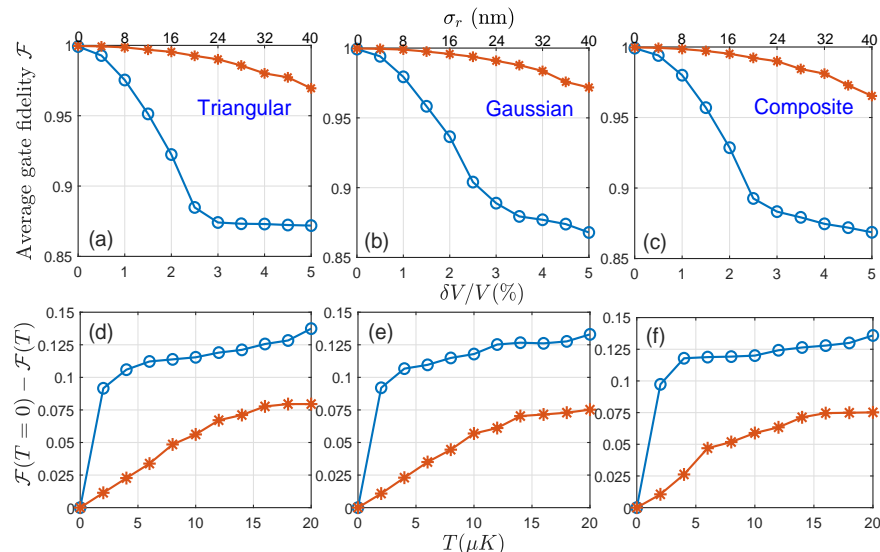


FIG. 3. (a-c) Average gate fidelity \mathcal{F} as a function of the deviation of interaction strength $\delta V/V \in [0, 0.05]$ (equivalent to the position deviation $\sigma_r \in [0, 40]$ nm), where the spontaneous decay from Rydberg levels are also considered. (d-f) Gate infidelity $\mathcal{F}(T=0) - \mathcal{F}(T)$ under different atomic temperatures T , which is treated as one of the resources to produce a deviation of interatomic interaction. Cases $q=0$ and $q \neq 0$ are presented by blue-line with circles and red-line with stars, respectively. Each point denotes an average of 300 random samplings.

It is well known that, a Rydberg antiblockade gate depends on the leading participation of double Rydberg states, and is thus more sensitive to the fluctuation of interatomic interaction than other gate mechanisms, such as Rydberg blockade [62–64] or adiabatic passage [65–71]. In practice this fluctuation in the relative position between two atoms can not be avoided, especially for two trapped atoms under a finite temperature [72]. That is the reason why the Rydberg antiblockade gates have not been reported by experiments. Although, e.g. placing two atoms at a long distance [73, 74] or lower the atomic temperature [75] can reduce the position error the robustness of antiblockade gates is still unsatisfactory.

In this section, to study the influence of interatomic position fluctuations, we first assume a relative deviation $\delta V/V$ to the non-fluctuated interaction strength V by obeying

$$V \rightarrow V(1 + \delta V/V) \quad (11)$$

where $\delta V/V$ stands for the maximal deviation amplitude. For each $\delta V/V$ a random value is generated within the range of $[-\delta V/V, \delta V/V]$ which adds to a small fluctuation in V . Fig.3(a-c) plot the average fidelity \mathcal{F} under different relative deviations with respect to the non-fluctuated value $\delta V/V \in [0, 0.05]$. Such deviation can also be characterized by the variation of two-atom distance [76] $\sigma_r = (\delta V/V)r_0/6$ due to $V = C_6/r_0^6$ considered for a van der Waals type interaction [77]. From Figs.3(a-c) it is apparent that, with a increasing deviation the SWAP gate fidelity significantly decreases for the $q=0$ case. E.g. when $\delta V/V = 0.05$ (equivalent to a position

deviation of $\sigma_r \approx 40$ nm), \mathcal{F} is decreased to about 0.87 with arbitrarily-optimized pulse shapes. However, with the help of the *modified antiblockade* condition where q is optimized to minimize the time-spent in $|rr\rangle$, the gate robustness against the deviation δV can be greatly improved. The average gate fidelity \mathcal{F} grows to be as high as 0.97 even in the case of a large distance deviation ~ 40 nm.

Accounting for the fact that deviation in the Rydberg interaction between two atoms usually comes from the imperfections of atomic cooling and trapping, we consider two atoms with a finite temperature T and re-calculate this position error. The relative position of two atoms satisfies a one-dimensional Gaussian distribution with its mean $r_0 = (C_6/V)^{1/6} \approx 4.8 \mu m$ and standard deviation $\sigma_r = \sqrt{k_B T / m \omega^2}$ varying with T . Here, k_B , m , ω mean the Boltzmann constant, the atomic mass and the trapping frequency. By assuming $\omega/2\pi = 147$ kHz, $T = 20 \mu K$ we can obtain $\sigma_r \approx 47.34$ nm and $\delta V/V \approx 5.92\%$. From the numerical results shown in Fig.3(d-f), it clear that, the gate infidelity $\mathcal{F}(T=0) - \mathcal{F}(T)$ (exclude the decay error) for the *modified antiblockade* case is dramatically decreased. At $T = 20 \mu K$ accessible by a typical cold-atom experiment [78], we find the gate infidelity due to the position error can sustain $\sim 7.5 \times 10^{-2}$, which is almost a 50% reduction as compared to that for the $q=0$ case. Among the existing approaches for achieving Rydberg antiblockade gates [30, 79, 80], our scheme presents the gate with the best position-error tolerance making one-step closer to the experimental demonstration of such antiblockade gates.

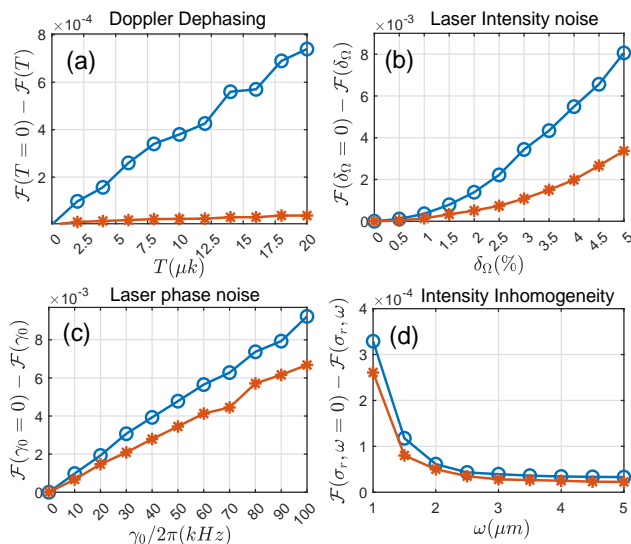


FIG. 4. Gate infidelity of the antiblockade SWAP gate with a pair of Gaussian optimal pulses (*Case ii*), caused by (a) Doppler dephasing under different atomic temperatures $T \in [0, 20]$ μK , (b) laser intensity fluctuations $\delta_\Omega \in [0, 0.05]$, (c) laser phase fluctuations (characterized by a dephasing rate $\gamma_0/2\pi \in [0, 100]$ kHz for the ground-Rydberg transitions), and (d) laser beam waist $\omega \in [1, 5]$ μm where the standard deviation of atomic position is fixed to $\sigma_r \approx 47.34$ nm considered for $T = 20$ μK . Similar to Fig.3 each point is obtained by an average of 300 random samplings.

V. ROBUSTNESS AGAINST TECHNICAL IMPERFECTIONS

In this section we study the gate infidelity by taking account of other technical imperfections as considered for a typical Rydberg experiment [81]. We will limit our discussions to the optimal Gaussian waveform (*Case ii*) which possesses a more smooth adjustment of the Rabi frequency as well as the best non-fluctuated gate fidelity. Except for the position error having explored in Sec. IV, other technical obstacles to a higher gate fidelity include the Doppler effect due to the atoms having a certain speed, the intensity and phase noises in excitation laser pulses, the relative position of atoms within a finite laser spatial width *et.al.* [82]. In the following we will analyze in detail the influence of each contribution to the gate infidelity so as to obtain a conservative estimation for the gate performance.

Doppler dephasing.- In a practical environment the qubit atoms would have a certain speed due to the residual thermal motion arising the Doppler effect. The resulting laser frequency detuning felt by the atoms will be slightly different from its desired value $\bar{\alpha} = 0$, which gives rise to a modified one-atom Hamiltonian

$$\hat{\mathcal{H}}_j = \Omega_1 e^{-i(\Delta_1 + \alpha_1)t} |0_j\rangle\langle r_j| + \Omega_2 e^{-i(\Delta_2 + \alpha_2)t} |1_j\rangle\langle r_j| + \text{H.c} \quad (12)$$

where $\alpha_{1(2)} = \vec{k}_{1(2),eff} \cdot \vec{v}$ stands for an extra phase factor to the Rabi frequency and should fulfill an one-dimensional Gaussian distribution

$$f(\alpha_{1,2}) = \frac{1}{\sqrt{2\pi}\sigma_{\alpha_{1,2}}} e^{-\frac{(\alpha_{1,2} - \bar{\alpha})^2}{2\sigma_{\alpha_{1,2}}^2}} \quad (13)$$

with respect to the standard deviations $\sigma_{\alpha_1} = k_{1,eff} v_{rms}$ and $\sigma_{\alpha_2} = k_{2,eff} v_{rms}$. Temperature $T = 20$ μK corresponds to the one-dimensional rms velocity $v_{rms} = \sqrt{k_B T/m} \approx 44$ mm/s. In addition, we recall our setup shown in Fig.1 where the two-photon transitions of $|0\rangle \rightarrow |r\rangle$ and $|1\rangle \rightarrow |r\rangle$ are mediated by two different low-lying p states. Therefore the effective wavevectors are $k_{1,eff} = 8.76 \times 10^6$ m^{-1} , $k_{2,eff} = 5 \times 10^6$ m^{-1} , by assuming two excitation lasers with a counter-propagating configuration to minimize thermal Doppler shifts. That means for each measurement the extra frequency detuning $\alpha_{1,2}$ (except $\Delta_{1,2}$) of excitation lasers seen by the atoms is a random value extracted from a centered Gaussian distribution (13) with the maximal standard deviations $(\sigma_{\alpha_1}, \sigma_{\alpha_2}) = (0.383, 0.219)$ MHz. Numerical simulation of the full dynamics gives rise to the infidelity $\mathcal{F}(T=0) - \mathcal{F}(T)$ for the SWAP gate, as shown in Fig.4(a) *versus* atomic temperature T . By averaging over sufficient runs of measurement, it is explicit that, the gate infidelity based on *modified antiblockade* mechanism is dramatically reduced by one order of magnitude as compared with that for the *perfect antiblockade* case. The reason is that $\alpha_{1(2)}$ serves as an extra and fluctuated detuning in addition to $\Delta_{1(2)}$, and the presence of an optimal q also adds to the tolerance against the detuning deviation. We find that, at $T = 20$ μK the infidelity caused by the Doppler dephasing has been suppressed to a negligible level $\sim 3.8 \times 10^{-5}$ for the $q \neq 0$ case.

Laser intensity noise.- In general the laser intensity fluctuation coming from external technical weakness, will lead to the deviation of desired excitation probability. Especially a gate scheme that depends on numerical optimization, requires the accuracy of pulse shapes. Here we introduce a same relative deviation $\delta_\Omega = \delta\Omega/\Omega_{1,2}^{\text{max}}$ in the range of $\delta_\Omega \in [0, 0.05]$ with respect to the laser maxima $\Omega_{1,2}^{\text{max}}$. During each run of measurement the laser Rabi frequency $\Omega_{1(2)}(t)$ is fluctuated by a random quantity obtained from $[-\delta_\Omega, +\delta_\Omega]\Omega_{1(2)}^{\text{max}}$ while the pulse shape is unchanged. Fig.4(b) shows the dependence of the gate infidelity on the laser intensity fluctuation. By increasing the relative deviation δ_Ω to 5.0 %, the *modified antiblockade* case apparently has a better robustness to the laser intensity noise, although both cases show the gate infidelity preserves at the level of $\sim 10^{-3}$.

Laser phase noise.- The phases $\phi_{1,2}(t)$ to the laser Rabi frequency $\Omega_{1,2}(t)$ are random processes which should be characterized by a phase noise spectral density as a function of the Fourier frequency [83]. Since the laser phase noise caused by different frequencies involved in excitation lasers, would lead to dephasing of Rabi oscillations [84–86], we describe the average result of laser phase noise

by introducing an extra Lindblad superoperator $\hat{\mathcal{L}}_d[\rho]$ in the master equation (8)

$$\hat{\mathcal{L}}_d[\rho] = \frac{1}{2} \sum_{j=1}^4 [2\hat{\mathcal{L}}_{d_j} \hat{\rho} \hat{\mathcal{L}}_{d_j}^\dagger - (\hat{\mathcal{L}}_{d_j}^\dagger \hat{\mathcal{L}}_{d_j} \hat{\rho} + \hat{\rho} \hat{\mathcal{L}}_{d_j}^\dagger \hat{\mathcal{L}}_{d_j})] \quad (14)$$

with four dephasing channels expressed as

$$\begin{aligned} \hat{\mathcal{L}}_{d,1(2)} &= \sqrt{\frac{\gamma_0}{2}} (|r_{1(2)}\rangle\langle r_{1(2)}| - |0_{1(2)}\rangle\langle 0_{1(2)}|) \\ \hat{\mathcal{L}}_{d,3(4)} &= \sqrt{\frac{\gamma_0}{2}} (|r_{1(2)}\rangle\langle r_{1(2)}| - |1_{1(2)}\rangle\langle 1_{1(2)}|) \end{aligned}$$

and γ_0 means a common dephasing rate. Fig.4(c) predicts the relationship between gate infidelity and different dephasing rates γ_0 . For each γ_0 we adopt a random value in the range of $[0, \gamma_0]$ and calculate the average infidelity $\mathcal{F}(\gamma_0 = 0) - \mathcal{F}(\gamma_0)$ after running 300 samplings. We observe that the effect of phase noise is more influential than that of the intensity noise, and the *modified antiblockade* case also shows a slightly higher tolerance to it. For $\gamma_0/2\pi = 100$ kHz the gate infidelity can achieve 6.68×10^{-3} which also plays a non-negligible role as compared with the position error ($\sim 10^{-2}$).

Inhomogeneity in Rabi frequencies.- In the above discussions we treat the thermal fluctuations of interatomic position in one dimension which is also the propagation direction for two excitation lasers, e.g., see Fig.1 along \hat{z} . In fact since lasers also have finite beam waists, such thermal fluctuations will make the atoms deviate from the laser center in the $\hat{x} - \hat{y}$ plane. As a result the actual laser intensity seen by the atoms would deviate from its ideal value, arising a position-dependent Rabi frequency only in the $\hat{x} - \hat{y}$ plane. To this end the original time-dependent Rabi frequencies $\Omega_1(t)$ and $\Omega_2(t)$ should be modified by adding a space-dependent factor,

$$\Omega_{1,2}(t, x, y) = \Omega_{1,2}(t, 0) e^{-\frac{x^2}{\omega_x^2} - \frac{y^2}{\omega_y^2}} \quad (15)$$

where $\Omega_{1,2}(t, 0) = \Omega_{1,2}(t)$ treats as the central Rabi frequency, and $\omega_x = \omega_y = \omega$ is assumed to be a common beam waist. We have ignored the intensity inhomogeneity in \hat{z} direction because the position deviation σ_r of atoms is smaller than the Rayleigh length by orders of magnitude [82]. Furthermore position (x, y) of two atomic qubits in the $\hat{x} - \hat{y}$ plane is modeled by a two-dimension Gaussian function with standard deviation $\sigma = \sigma_x = \sigma_y \approx 47.34$ nm at $T = 20$ μ K. In Fig.4(d) we tune the beam waist ω in the range of $[1, 5]$ μ m to see the effect of intensity inhomogeneity. It is clear that both cases lead to similar gate infidelities due to their comparable laser intensities. When $\omega > 2.0$ μ m the influence can be lowered to $< 10^{-4}$. However if ω is narrowed to be below 1.0 μ m we find the infidelity has a dramatic increase because of the large intensity variations felt by the atoms when the beam waist is too small. While accounting for the fact that the excitation laser can be focused to a wide waist of ~ 10 μ m typically [87], this error can be totally negligible in the scheme.

TABLE II. Error budget for *Case ii* with Gaussian-type optimal pulses. As expected, among all obstacles (intrinsic and technical) the position error originating from fluctuations in the relative position between two atoms, is the dominant error source. The Doppler dephasing and the inhomogeneity in laser Rabi frequencies are relatively less important. Every error number is obtained via an average over 300 repeated measurements and the values in parenthesis denote the maximal deviation. By considering all error sources simultaneously we obtain a very conservative estimate for the gate fidelity, which are $\mathcal{F} \geq 0.8482$ and $\mathcal{F} \geq 0.9142$, corresponding to the cases of $q = 0$ and $q \neq 0$ respectively.

Error Sources	Error Budget	
	$q/2\pi$	
	0	5.037 MHz
Rydberg decay	7×10^{-4}	3×10^{-4}
Position fluctuation ($\sigma_r = 47.34$ nm)	1.33×10^{-1}	7.5×10^{-2}
Doppler dephasing ($T = 20$ μ K)	7.4×10^{-4}	3.8×10^{-5}
Inhomogeneous Rabi frequency ($\omega = 2$ μ m)	6.13×10^{-5}	5.02×10^{-5}
Laser intensity ($\delta_\Omega = 5.0$ %)	8.06×10^{-3}	3.37×10^{-3}
Laser phase ($\gamma_0/2\pi = 100$ kHz)	9.23×10^{-3}	6.68×10^{-3}

VI. DISCUSSION AND CONCLUSION

Ever since the pioneering works [88, 89] proposed the idea of quantum computation with neutral atoms a large number of groups have focused on the experimental demonstration of various Rydberg quantum gates via *Rydberg blockade* [90–92]. This method serves as the leading mainstream blueprint mainly because of its powerful insensitivity to the variation of interatomic interactions that fundamentally makes the position error negligible [56]. In addition, another set of universal quantum gates based on *Rydberg antiblockade* effect also emerges, since the first scheme by Carr and Saffman proposed a new method for preparing Rydberg entangled states via the combination of dissipative dynamics and antiblockade [8]. Nevertheless, such antiblockade gates require an exact knowledge of the interaction strength V , and thus are sensitive to the interaction deviation δV in practice. In this work we restrict our attention to the implementation of a two-qubit SWAP gate based on antiblockade mechanism, and show that it is possible to improve the tolerance of gates to the position error caused by e.g. residual thermal motion of atoms in the trapping region.

Table II summarizes the gate error budgeting of our protocol under different practical imperfections. Among them, although the dominant gate error remains the position fluctuation, e.g. it stays at the level of 10^{-2} for the $q \neq 0$ case; yet this value has been greatly decreased by at least one order of magnitude as compared with that in the reported antiblockade-gate schemes [30, 79, 80, 93]. Besides our protocol suffers a relatively larger sensitivity $\sim 10^{-3}$ to the fluctuation of excitation lasers because of

the pulse optimization [94]. Other errors due to finite radiative lifetime of Rydberg states, the Doppler dephasing as well as the inhomogeneous Rabi frequency, are all contributing negligible $10^{-5} \sim 10^{-4}$. After taking into account all error sources we can obtain a more conservative lower bound on the predicted gate fidelity which is $\mathcal{F} \geq 0.9142$. The potential for a higher-fidelity antiblockade gate can depend on a further improvement in the tolerance to the position fluctuation, by using cooling method. E.g. an antiblockade SWAP gate with fidelity larger than 0.9814 is possible while cooling atomic qubits to 1.5 μK below. Because the position error can be reduced to about 8.2×10^{-3} there.

In conclusion we have shown the *modified antiblockade* effect incorporating with pulse optimization, can lead to Rydberg antiblockade SWAP gates with unprecedented tolerance, arising the experimental demonstration for them with great promise. Through optimization we find the time-spent in the double Rydberg state can be reduced by more than 70% which does not depend on the realistic shape of the laser pulses. For this reason the insensitivity of such gates to the position fluctuations can be improved by one order of magnitude, arising a quite competitive gate fidelity of $\mathcal{F} \geq 0.9142$ in the presence of significant position deviation for a practical temperature $T \sim 20 \mu\text{K}$. Larger gate tolerance is achievable either by using more adequate cooling techniques [95], optimal three-dimension geometric configurations [96], or fault-tolerant optimization algorithm [97]. The prospect for realizing fast and high-fidelity swapping of arbitrary initialization requiring stronger laser Rabi frequencies $\sim 2\pi \times 50$ MHz as presented in appendix B, may give rise to more important applications of the SWAP gates in the frontier of quantum information science.

ACKNOWLEDGMENTS

We acknowledge financial support by the NSFC under Grants No. 12174106, No.11474094, No.11104076, No.12274376, No.12304407, by the Science and Technology Commission of Shanghai Municipality under Grant No.18ZR1412800.

Appendix A: Derivation of effective Hamiltonian Eqs.(4-6)

In this appendix, we derive the effective Hamiltonians in Eqs.(4-6). We recall the full Hamiltonian for our two-qubit SWAP gate, as

$$\hat{\mathcal{H}} = \hat{\mathcal{H}}_1 \otimes \hat{I}_2 + \hat{I}_1 \otimes \hat{\mathcal{H}}_2 + \hat{V}_{rr} \quad (\text{A1})$$

with \hat{I}_j denoting a 3×3 identity matrix and $j = 1, 2$. In the interaction picture the Hamiltonian of single atom reads

$$\hat{\mathcal{H}}_j = \Omega_1 e^{-i\Delta_1 t} |0_j\rangle\langle r_j| + \Omega_2 e^{-i\Delta_2 t} |1_j\rangle\langle r_j| + \text{H.c} \quad (\text{A2})$$

and

$$\hat{V}_{rr} = U_{rr} |rr\rangle\langle rr| \quad (\text{A3})$$

is the Rydberg-mediated interaction and $U_{rr} = \Delta_1 + \Delta_2 + q$. Note that q is a tunable factor which modifies the *perfect antiblockade* condition.

Turning into the frame of two-atom basis states $\{|00\rangle, |01\rangle, |0r\rangle, |10\rangle, |11\rangle, |1r\rangle, |r0\rangle, |r1\rangle, |rr\rangle\}$ all Hamiltonians $\hat{\mathcal{H}}_1, \hat{\mathcal{H}}_2, \hat{V}_{rr}$ should be re-expressed as

$$\begin{aligned} \hat{\mathcal{H}}_1 &= \Omega_1 e^{-i\Delta_1 t} (|r1\rangle\langle 01| + |r0\rangle\langle 00| + |rr\rangle\langle 0r|) \\ &\quad + \Omega_2 e^{-i\Delta_2 t} (|r1\rangle\langle 11| + |r0\rangle\langle 10| + |rr\rangle\langle 1r|) + \text{H.c.} \\ \hat{\mathcal{H}}_2 &= \Omega_1 e^{-i\Delta_1 t} (|1r\rangle\langle 10| + |0r\rangle\langle 00| + |rr\rangle\langle r0|) \\ &\quad + \Omega_2 e^{-i\Delta_2 t} (|1r\rangle\langle 11| + |0r\rangle\langle 01| + |rr\rangle\langle r1|) + \text{H.c.} \\ \hat{V}_{rr} &= (\Delta_1 + \Delta_2 + q) |rr\rangle\langle rr| \end{aligned} \quad (\text{A4})$$

with which the full Hamiltonian (A1) of system simplifies into

$$\hat{\mathcal{H}} = \hat{\mathcal{H}}_1 + \hat{\mathcal{H}}_2 + \hat{V}_{rr}. \quad (\text{A5})$$

To demonstrate the role of Rydberg-mediated interaction we rotate the full Hamiltonian $\hat{\mathcal{H}}$ with respect to the unitary operator

$$\hat{U} = e^{i(\Delta_1 + \Delta_2) |rr\rangle\langle rr| t} \quad (\text{A6})$$

which leads to

$$\hat{\mathcal{H}}' = \hat{U}^\dagger \hat{\mathcal{H}} \hat{U} - i\hbar \hat{U}^\dagger \frac{\partial \hat{U}}{\partial t} \quad (\text{A7})$$

in the rotation frame. We find the product $\hat{\mathcal{H}}'$ composes two parts: $\hat{\mathcal{H}}' = \hat{\mathcal{H}}_0 + \hat{\mathcal{H}}_I$. The first term is

$$\begin{aligned} \hat{\mathcal{H}}_0 &= \Omega_1 e^{-i\Delta_1 t} (|r1\rangle\langle 01| + |r0\rangle\langle 00|) + \Omega_1 e^{i\Delta_2 t} |rr\rangle\langle 0r| \\ &\quad + \Omega_2 e^{-i\Delta_2 t} (|r1\rangle\langle 11| + |r0\rangle\langle 10|) + \Omega_2 e^{i\Delta_1 t} |rr\rangle\langle 1r| \\ &\quad + \Omega_2 e^{-i\Delta_2 t} (|0r\rangle\langle 01| + |1r\rangle\langle 11|) + \Omega_2 e^{i\Delta_1 t} |rr\rangle\langle r1| \\ &\quad + \Omega_1 e^{-i\Delta_1 t} (|0r\rangle\langle 00| + |1r\rangle\langle 10|) + \Omega_1 e^{i\Delta_2 t} |rr\rangle\langle r0| + \text{H.c} \end{aligned}$$

while the second one is

$$\hat{\mathcal{H}}_I = q |rr\rangle\langle rr| \quad (\text{A8})$$

Next note that the Hamiltonian $\hat{\mathcal{H}}_0$ in the interaction picture can be exactly rewritten as a more universal form

$$\hat{\mathcal{H}}_0 = \sum_{n=1,2} \hat{h}_n^\dagger e^{i\Delta_n t} + \hat{h}_n e^{-i\Delta_n t} \quad (\text{A9})$$

where

$$\begin{aligned} \hat{h}_1 &= \Omega_1 (|r1\rangle\langle 01| + |r0\rangle\langle 00| + |0r\rangle\langle 00| + |1r\rangle\langle 10|) \\ &\quad + \Omega_2 (|1r\rangle\langle rr| + |r1\rangle\langle rr|) \\ \hat{h}_2 &= \Omega_2 (|0r\rangle\langle 01| + |1r\rangle\langle 11| + |r1\rangle\langle 11| + |r0\rangle\langle 10|) \\ &\quad + \Omega_1 (|0r\rangle\langle rr| + |r0\rangle\langle rr|). \end{aligned} \quad (\text{A10})$$

Especially, when $|\Delta_1| \gg \Omega_1$ and $|\Delta_2| \gg \Omega_2$ we can further deduce the effective form of $\hat{\mathcal{H}}_0$ by ignoring the high-frequency oscillation terms under the rotating-wave approximation, which yields [98]

$$\hat{\mathcal{H}}_{0,eff} = \frac{1}{\Delta_1}[\hat{h}_1^\dagger, \hat{h}_1] + \frac{1}{\Delta_2}[\hat{h}_2^\dagger, \hat{h}_2] \quad (\text{A11})$$

$$\begin{aligned} \hat{\mathcal{H}}_{0,eff} = & -\left(\frac{\Omega_1^2}{\Delta_1} + \frac{\Omega_1^2}{\Delta_2}\right)|r0\rangle\langle 0r| - \left(\frac{\Omega_1^2}{\Delta_1} + \frac{\Omega_1^2 + \Omega_2^2}{\Delta_2}\right)(|r0\rangle\langle r0| + |0r\rangle\langle 0r|) - \left(\frac{\Omega_2^2}{\Delta_1} + \frac{\Omega_2^2}{\Delta_2}\right)|r1\rangle\langle 1r| \\ & - \left(\frac{\Omega_2^2}{\Delta_2} + \frac{\Omega_1^2 + \Omega_2^2}{\Delta_1}\right)(|r1\rangle\langle r1| + |1r\rangle\langle 1r|) + \left(\frac{\Omega_1\Omega_2}{\Delta_1} + \frac{\Omega_1\Omega_2}{\Delta_2}\right)(|rr\rangle\langle 01| + |rr\rangle\langle 10|) \\ & + \left(\frac{\Omega_1^2}{\Delta_1} + \frac{\Omega_2^2}{\Delta_2}\right)(|01\rangle\langle 01| + |10\rangle\langle 10|) + \frac{2\Omega_1^2}{\Delta_1}|00\rangle\langle 00| + \frac{2\Omega_2^2}{\Delta_2}|11\rangle\langle 11| + \left(\frac{2\Omega_2^2}{\Delta_1} + \frac{2\Omega_1^2}{\Delta_2}\right)|rr\rangle\langle rr| + \text{H.c.} \end{aligned} \quad (\text{A12})$$

Following Eq.(A12) we observe that the single Rydberg states such as $\{|0r\rangle, |r0\rangle, |1r\rangle, |r1\rangle\}$ are decoupled to the initial-state space which is only composed by $\{|00\rangle, |01\rangle, |10\rangle, |11\rangle\}$. So it is safe to drop these trivial terms and the full Hamiltonian $\hat{\mathcal{H}}'$ takes an effective form as

$$\begin{aligned} \hat{\mathcal{H}}'_{eff} = & \left(\frac{\Omega_1\Omega_2}{\Delta_1} + \frac{\Omega_1\Omega_2}{\Delta_2}\right)(|rr\rangle\langle 01| + |rr\rangle\langle 10|) \quad (\text{A13}) \\ & + \left(\frac{\Omega_1^2}{\Delta_1} + \frac{\Omega_2^2}{\Delta_2}\right)(|01\rangle\langle 01| + |10\rangle\langle 10|) + \frac{2\Omega_1^2}{\Delta_1}|00\rangle\langle 00| \\ & + \frac{2\Omega_2^2}{\Delta_2}|11\rangle\langle 11| + \left(\frac{2\Omega_2^2}{\Delta_1} + \frac{2\Omega_1^2}{\Delta_2} + q\right)|rr\rangle\langle rr| + \text{H.c.} \end{aligned}$$

Hence when the initial state is $|00\rangle$ or $|11\rangle$ the system stays decoupled because

$$\hat{\mathcal{H}}_{00,eff} = \frac{2\Omega_1^2}{\Delta_1}|00\rangle\langle 00| \text{ or } \hat{\mathcal{H}}_{11,eff} = \frac{2\Omega_2^2}{\Delta_2}|11\rangle\langle 11| \quad (\text{A14})$$

However, when the initial state is $|01\rangle$ (equivalent to $|10\rangle$) the effective Hamiltonian becomes

$$\begin{aligned} \hat{\mathcal{H}}_{01,eff} = & \left(\frac{\Omega_1\Omega_2}{\Delta_1} + \frac{\Omega_1\Omega_2}{\Delta_2}\right)(|rr\rangle\langle 01| + |01\rangle\langle rr|) + \text{H.c.} \\ & + \left(\frac{\Omega_1^2}{\Delta_1} + \frac{\Omega_2^2}{\Delta_2}\right)(|01\rangle\langle 01| + |10\rangle\langle 10|) \\ & + \left(\frac{2\Omega_2^2}{\Delta_1} + \frac{2\Omega_1^2}{\Delta_2} + q\right)|rr\rangle\langle rr| \quad (\text{A15}) \end{aligned}$$

It is worthwhile to stress that although the effective Hamiltonian (A15) only involves the swapping between $|01\rangle$ and $|10\rangle$; yet it is clearly mediated by the double Rydberg state $|rr\rangle$ arising its sensitivity to the position error. Luckily the presence of factor $q(\neq 0)$ in the last term adds to an extra detuning to make the double excitation state $|rr\rangle$ off-resonance which strongly suppresses the population on it. The resulting gate is insusceptible to the interaction fluctuation. In addition we identify that, although the ac Stark shifts to the ground states $|01\rangle$ and

By inserting Eq.(A10) into (A11) the effective Hamiltonian takes form of

$|10\rangle$ could be overcome by e.g. applying auxiliary atom-field couplings which increases experimental difficulties [49], the way of pulse optimization can largely suppress this influence, promising for a high-fidelity SWAP gate with improved robustness [99].

Appendix B: Application: Fast arbitrary initialization swapping

In this appendix we provide calculations for a fast two-qubit SWAP gate with arbitrary initialization. By reducing the gate time to be $T_g = 0.1 \mu\text{s}$ which requires a larger Rabi frequency approximately $2\pi \times 50 \text{ MHz}$, we perform deep parameter optimization towards the minimization of time-spent in double Rydberg state which finally leads to a new set of optimal parameters in this case:

$$\begin{aligned} \Omega_1^{\max}/2\pi &= 42.18 \text{ MHz}, \Omega_2^{\max}/2\pi = 53.93 \text{ MHz} \\ q/2\pi &= 42.64 \text{ MHz}, \Delta_1/2\pi = -95.57 \text{ MHz} \\ \omega_1 &= 0.038 \mu\text{s}, \omega_2 = 0.1275 \mu\text{s} \end{aligned}$$

In order to show the performance of a fast SWAP gate we introduce a normalized two-qubit state as the initial state which is

$$|\Psi(0)\rangle = A_{00}|00\rangle + A_{01}|01\rangle + A_{10}|10\rangle + A_{11}|11\rangle \quad (\text{B1})$$

with $\sum_{i,j} |A_{i,j}|^2 = 1$ and $i, j \in \{0, 1\}$. Such arbitrariness of the initial state can be used to explore the fast state swapping of the scheme. For an arbitrary initialization the ideal output state is $|\Psi(T_g)\rangle = A_{00}|00\rangle + A_{10}|01\rangle + A_{01}|10\rangle + A_{11}|11\rangle$. Here we modify the definition of average fidelity in Eq.(10) by following

$$\mathcal{F} = \text{Tr} \sqrt{\sqrt{U} \rho(t = T_g) \sqrt{U}} \quad (\text{B2})$$

because the initial state $|\Psi(0)\rangle$ is individually normalized. ρ is the practical density matrix at time $t = T_g$ and

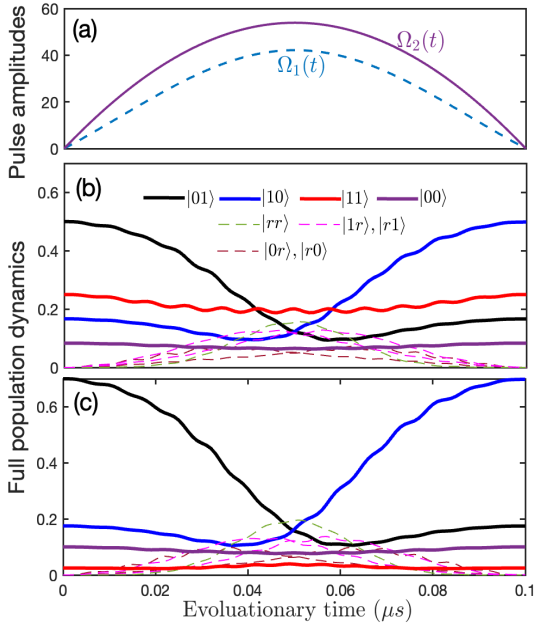


FIG. 5. Full population dynamics based on arbitrary initialization within a shorter gate duration $T_g = 0.1 \mu\text{s}$. (a) Optimal Gaussian laser shapes $\Omega_1(t), \Omega_2(t)$ and (b) $A_{00} = \frac{1}{\sqrt{12}}$, $A_{01} = \frac{1}{\sqrt{2}}$, $A_{10} = \frac{1}{\sqrt{6}}$, $A_{11} = \frac{1}{\sqrt{4}}$ and (c) $A_{00} = \frac{1}{\sqrt{10}}$, $A_{01} = \sqrt{\frac{7}{10}}$, $A_{10} = \sqrt{\frac{7}{40}}$, $A_{11} = \frac{1}{\sqrt{40}}$. All linetypes are described in the figure.

$U = |\Psi(0)\rangle\langle\Psi(0)|$ is the ideal SWAP matrix for arbitrary input state.

For comparison we plot the full population dynamics of each intermediate state in Fig.5(b-c) based on two specific examples and the corresponding Gaussian pulses(optimal) are given in Fig.5(a). One could see from Fig.5(b-c) that, although a fast($\sim 0.1 \mu\text{s}$) and high-fidelity(> 0.99) state swapping can be achieved for both cases the fidelities have a slight decrease when initial population $|A_{01}|^2 + |A_{10}|^2$ grows. Because if the initial state is largely populated in $|01\rangle$ or $|10\rangle$ the time-spent in the double Rydberg state would increase arising a larger decay error. Therefore we find the ideal fidelity \mathcal{F} reaches 0.9991[(b)] and 0.9988[(c)] considered for a non-fluctuated environment. Whereas, as taking account of the technical limitations from a typical Rydberg setup we find the laser intensity noise has the greatest influence ($\sim 10^{-2}$) because of the larger Rabi frequency required for a submicrosecond gate time. In contrast the infidelity caused by the position fluctuation of atoms has been reduced to a scale of $\sim 10^{-4}$ due to the smaller time-spent in $|rr\rangle$. After accounting for all technical noises the predicted fidelity for fast state swapping can reach about 0.9845 and 0.9809 for these two cases. It is worthwhile to note that, since the effective coupling strength between ground and Rydberg states remains about $2\pi \times (1 \sim 10)$ MHz typically, achieving fast quantum state operations within a submicrosecond gate time still needs more efforts in the future.

-
- [1] M. Saffman, Quantum computing with atomic qubits and rydberg interactions: progress and challenges, *Journal of Physics B: Atomic, Molecular and Optical Physics* 49, 202001 (2016).
 - [2] L. Henriot, L. Beguin, A. Signoles, T. Lahaye, A. Browaeys, G.-O. Reymond, and C. Jurczak, Quantum computing with neutral atoms, *Quantum* 4, 327 (2020).
 - [3] M. Morgado and S. Whitlock, Quantum simulation and computing with rydberg-interacting qubits, *AVS Quantum Science* 3 (2021).
 - [4] I. Cong, H. Levine, A. Keesling, D. Bluvstein, S.-T. Wang, and M. D. Lukin, Hardware-efficient, fault-tolerant quantum computation with rydberg atoms, *Physical Review X* 12, 021049 (2022).
 - [5] X.-F. Shi, Quantum logic and entanglement by neutral rydberg atoms: methods and fidelity, *Quantum Science and Technology* 7, 023002 (2022).
 - [6] C. Dlaska, K. Ender, G. B. Mbeng, A. Kruckenhauser, W. Lechner, and R. van Bijnen, Quantum optimization via four-body rydberg gates, *Physical Review Letters* 128, 120503 (2022).
 - [7] T. Graham, Y. Song, J. Scott, C. Poole, L. Phuttitarn, K. Jooya, P. Eichler, X. Jiang, A. Marra, B. Grinkemeyer *et al.*, Multi-qubit entanglement and algorithms on a neutral-atom quantum computer, *Nature* 604, 457 (2022).
 - [8] A. Carr and M. Saffman, Preparation of entangled and antiferromagnetic states by dissipative rydberg pumping, *Physical Review Letters* 111, 033607 (2013).
 - [9] X.-Q. Shao, J.-B. You, T.-Y. Zheng, C. Oh, and S. Zhang, Stationary three-dimensional entanglement via dissipative rydberg pumping, *Physical Review A* 89, 052313, (2014).
 - [10] S.-L. Su, Q. Guo, H.-F. Wang, and S. Zhang, Simplified scheme for entanglement preparation with rydberg pumping via dissipation, *Physical Review A* 92, 022328, (2015).
 - [11] G. Barontini, L. Hohmann, F. Haas, J. Estève, and J. Reichel, Deterministic generation of multiparticle entanglement by quantum zeno dynamics, *Science* 349, 1317 (2015).
 - [12] X. Chen, H. Xie, G.-W. Lin, X. Shang, M.-Y. Ye, and X.-M. Lin, Dissipative generation of a steady three-atom singlet state based on rydberg pumping, *Physical Review A* 96, 042308 (2017).
 - [13] Y.-H. Chen, Z.-C. Shi, J. Song, Y. Xia, and S.-B. Zheng, Accelerated and noise-resistant generation of high-fidelity steady-state entanglement with rydberg atoms, *Physical Review A* 97, 032328 (2018).
 - [14] T. M. Wintermantel, Y. Wang, G. Lochead, S. Shevate, G. Brennen, and S. Whitlock, Unitary and nonunitary quantum cellular automata with rydberg arrays, *Physical Review Letters* 124, 070503 (2020).
 - [15] F. M. Gambetta, C. Zhang, M. Hennrich, I. Lesanovsky, and W. Li, Long-range multibody interactions and three-body antiblockade in a trapped rydberg ion chain, *Phys-*

- ical Review Letters* 125, 133602 (2020).
- [16] S. K. Mallavarapu, A. Niranjan, W. Li, S. Wüster, and R. Nath, Population trapping in a pair of periodically driven rydberg atoms, *Physical Review A* 103 023335 (2021).
- [17] M. Malinowski, C. Zhang, V. Negnevitsky, I. Rojkov, F. Reiter, T.-L. Nguyen, M. Stadler, D. Kienzler, K. K. Mehta, and J. P. Home, Generation of a maximally entangled state using collective optical pumping, *Physical Review Letters* 128, 080503 (2022).
- [18] T. P. C. Ates, T. Pohl and J.M.Rost, Antiblockade in rydberg excitation of an ultracold lattice gas, *Physical Review Letters* 98, 023002 (2007).
- [19] T. Amthor, C. Giese, C. S. Hofmann, and M. Weidemüller, Evidence of antiblockade in an ultracold rydberg gas, *Physical Review Letters* 104, 013001 (2010).
- [20] S. Bai, X. Tian, X. Han, Y. Jiao, J. Wu, J. Zhao, and S. Jia, Distinct antiblockade features of strongly interacting rydberg atoms under a two-color weak excitation scheme, *New Journal of Physics* 22, 013004 (2020).
- [21] T. Xing, X. Wu, and G. Xu, Nonadiabatic holonomic three-qubit controlled gates realized by one-shot implementation, *Physical Review A* 101, 012306 (2020).
- [22] M. Saffman and T. Walker, Analysis of a quantum logic device based on dipole-dipole interactions of optically trapped rydberg atoms, *Physical Review A* 72, 022347 (2005).
- [23] W. Li, C. Ates, and I. Lesanovsky, Nonadiabatic motional effects and dissipative blockade for rydberg atoms excited from optical lattices or microtraps, *Physical Review Letters* 110 213005 (2013).
- [24] X.-F. Shi and T. Kennedy, Annulled van der waals interaction and fast rydberg quantum gates, *Physical Review A* 95, 043429 (2017).
- [25] F. Robicheaux, T. Graham, and M. Saffman, Photon-recoil and laser-focusing limits to rydberg gate fidelity, *Physical Review A* 103, 022424 (2021).
- [26] S. De Léséleuc, D. Barredo, V. Lienhard, A. Browaeys, and T. Lahaye, Analysis of imperfections in the coherent optical excitation of single atoms to rydberg states, *Physical Review A* 97, 053803 (2018).
- [27] F. Yang, Y.-C. Liu, and L. You, Atom-photon spin-exchange collisions mediated by rydberg dressing, *Physical Review Letters* 125, 143601 (2020).
- [28] F. M. Gambetta, W. Li, F. Schmidt-Kaler, and I. Lesanovsky, Engineering nonbinary rydberg interactions via phonons in an optical lattice, *Physical Review Letters* 124, 043402 (2020).
- [29] S.-L. Su, Y. Tian, H. Shen, H. Zang, E. Liang, and S. Zhang, Applications of the modified rydberg antiblockade regime with simultaneous driving, *Physical Review A* 96, 042335, (2017).
- [30] J.-L. Wu, Y. Wang, J.-X. Han, Y.-K. Feng, S.-L. Su, Y. Xia, Y. Jiang, and J. Song, One-step implementation of rydberg-antiblockade swap and controlled-swap gates with modified robustness, *Photonics Research* 9, 814 (2021).
- [31] A. M. Kaufman, B. J. Lester, and C. A. Regal, Cooling a single atom in an optical tweezer to its quantum ground state, *Physical Review X* 2, 041014, (2012).
- [32] J. Hu, A. Urvoy, Z. Vendeiro, V. Crépel, W. Chen, and V. Vuletić, Creation of a bose-condensed gas of 87rb by laser cooling, *Science* 358, 1078 (2017).
- [33] C. Hölzl, A. Götzelmann, M. Wirth, M. S. Safronova, S. Weber, and F. Meinert, Motional ground-state cooling of single atoms in state-dependent optical tweezers, *Physical Review Research* 5, 033093 (2023).
- [34] J. Yang, X. He, R. Guo, P. Xu, K. Wang, C. Sheng, M. Liu, J. Wang, A. Derevianko, and M. Zhan, Coherence preservation of a single neutral atom qubit transferred between magic-intensity optical traps, *Physical Review Letters* 117, 123201 (2016).
- [35] Y. Sun, P. Xu, P.-X. Chen, and L. Liu, Controlled phase gate protocol for neutral atoms via off-resonant modulated driving, *Physical Review Applied* 13, 024059 (2020).
- [36] A. Pagano, S. Weber, D. Jaschke, T. Pfau, F. Meinert, S. Montangero, and H. P. Büchler, Error budgeting for a controlled-phase gate with strontium-88 rydberg atoms, *Physical Review Research* 4, 033019 (2022).
- [37] W. Feng and D. wei Wang, Quantum fredkin gate based on synthetic three-body interactions in superconducting circuits, *Physical Review A*, 101, 062312 (2020).
- [38] M. Riebe, T. Monz, K. Kim, A. Villar, P. Schindler, M. Chwalla, M. Hennrich, and R. Blatt, Deterministic entanglement swapping with an ion-trap quantum computer, *Nature Physics* 4, 839 (2008).
- [39] X.-s. Ma, S. Zotter, J. Kofler, R. Ursin, T. Jennewein, Č. Brukner, and A. Zeilinger, Experimental delayed-choice entanglement swapping, *Nature Physics* 8, 479 (2012).
- [40] W. Ning, X.-J. Huang, P.-R. Han, H. Li, H. Deng, Z.-B. Yang, Z.-R. Zhong, Y. Xia, K. Xu, D. Zheng *et al.*, Deterministic entanglement swapping in a superconducting circuit, *Physical Review Letters* 123, 060502 (2019).
- [41] N. Sangouard, C. Simon, H. De Riedmatten, and N. Gisin, Quantum repeaters based on atomic ensembles and linear optics, *Reviews of Modern Physics* 83, 33 (2011).
- [42] I. J. Tillman, A. Rubenok, S. Guha, and K. P. Seshadreesan, Supporting multiple entanglement flows through a continuous-variable quantum repeater, *Physical Review A* 106, 062611 (2022).
- [43] Y. K. Chahine, I. R. Nemitz, and J. D. Lekki, Protocol for suppression of noise from stimulated multiphoton emissions in concatenated entanglement swapping links and quantum repeaters, *Physical Review A* 108, 022609 (2023).
- [44] H. Levine, A. Keesling, G. Semeghini, A. Omran, T. T. Wang, S. Ebadi, H. Bernien, M. Greiner, V. Vuletić, H. Pichler, and M. D. Lukin, Parallel implementation of high-fidelity multiqubit gates with neutral atoms, *Physical Review Letters* 123, 170503 (2019).
- [45] N. Šibalić, J. D. Pritchard, C. S. Adams, and K. J. Weatherill, Arc: An open-source library for calculating properties of alkali rydberg atoms, *Computer Physics Communications* 220, 319 (2017).
- [46] W. Lee, M. Kim, H. Jo, Y. Song, and J. Ahn, Coherent and dissipative dynamics of entangled few-body systems of rydberg atoms, *Physical Review A* 99, 043404 (2019).
- [47] F. Liu, Z.-C. Yang, P. Bienias, T. Iadecola, and A. V. Gorshkov, Localization and criticality in antiblockaded two-dimensional rydberg atom arrays, *Physical Review Letters* 128,013603 (2022).
- [48] M. Magoni, R. Joshi, and I. Lesanovsky, Molecular dynamics in rydberg tweezer arrays: Spin-phonon entanglement and jahn-teller effect, *Physical Review Letters* 131, 093002 (2023).
- [49] S.-L. Su, E. Liang, S. Zhang, J.-J. Wen, L.-L. Sun, Z. Jin,

- and A.-D. Zhu, One-step implementation of the rydberg-rydberg-interaction gate, *Physical Review A* 93, 012306 (2016).
- [50] M. H. Goerz, E. J. Halperin, J. M. Aytac, C. P. Koch, and K. B. Whaley, Robustness of high-fidelity rydberg gates with single-site addressability, *Physical Review A* 90, 032329 (2014).
- [51] K. McDonnell, L. F. Keary, and J. D. Pritchard, Demonstration of a quantum gate using electromagnetically induced transparency, *Physical Review Letters* 129, 200501 (2022).
- [52] M. Mohan, R. de Keijzer, and S. Kokkelmans, Robust control and optimal rydberg states for neutral atom two-qubit gates, *Physical Review Research* 5, 033052 (2023).
- [53] X. Jiang, J. Scott, M. Friesen, and M. Saffman, Sensitivity of quantum gate fidelity to laser phase and intensity noise, *Physical Review A* 107, 042611 (2023).
- [54] R. Li, J. Qian, and W. Zhang, Proposal for practical rydberg quantum gates using a native two-photon excitation, *Quantum Science and Technology* 8, 035032 (2023).
- [55] E. Braaten, H.-W. Hammer, and G. P. Lepage, Lindblad equation for the inelastic loss of ultracold atoms, *Physical Review A* 95, 012708 (2017).
- [56] L. S. Theis, F. Motzoi, F. K. Wilhelm, and M. Saffman, High-fidelity rydberg-blockade entangling gate using shaped, analytic pulses, *Physical Review A* 94, 032306 (2016).
- [57] J.-L. Wu, S.-L. Su, Y. Wang, J. Song, Y. Xia, and Y.-Y. Jiang, Effective rabi dynamics of rydberg atoms and robust high-fidelity quantum gates with a resonant amplitude-modulation field, *Optics Letters* 45, 1200 (2020).
- [58] Z. Fu, P. Xu, Y. Sun, Y.-Y. Liu, X.-D. He, X. Li, M. Liu, R.-B. Li, J. Wang, L. Liu, and M.-S. Zhan, High-fidelity entanglement of neutral atoms via a rydberg-mediated single-modulated-pulse controlled-phase gate, *Physical Review A* 105, 042430 (2022).
- [59] X. Li, X. Shao, and W. Li, Single temporal-pulse-modulated parameterized controlled-phase gate for rydberg atoms, *Physical Review Applied* 18, 044042 (2022).
- [60] M. Reetz-Lamour, T. Amthor, J. Deiglmayr, and M. Weidemüller, Rabi oscillations and excitation trapping in the coherent excitation of a mesoscopic frozen rydberg gas, *Physical Review Letters* 100, 253001 (2008).
- [61] J. D. Thompson, T. G. Tiecke, A. S. Zibrov, V. Vuletić, and M. D. Lukin, Coherence and raman sideband cooling of a single atom in an optical tweezer, *Physical Review Letters* 110, 133001 (2013).
- [62] D. Møller, L. B. Madsen, and K. Mølmer, Quantum gates and multiparticle entanglement by rydberg excitation blockade and adiabatic passage, *Physical Review Letters* 100, 170504 (2008).
- [63] L. Isenhower, E. Urban, X. L. Zhang, A. T. Gill, T. Henage, T. A. Johnson, T. G. Walker, and M. Saffman, Demonstration of a neutral atom controlled-quantum gate, *Physical Review Letters* 104, 010503 (2010).
- [64] T. Wilk, A. Gaëtan, C. Evellin, J. Wolters, Y. Miroshnychenko, P. Grangier, and A. Browaeys, Entanglement of two individual neutral atoms using rydberg blockade, *Physical Review Letters* 104, 010502 (2010).
- [65] D. D. B. Rao and K. Mølmer, Robust rydberg-interaction gates with adiabatic passage, *Physical Review A* 89, 030301 (2014).
- [66] I. I. Beterov, M. Saffman, E. A. Yakshina, D. B. Tretyakov, V. M. Entin, S. Bergamini, E. A. Kuznetsova, and I. I. Ryabtsev, Two-qubit gates using adiabatic passage of the stark-tuned förster resonances in rydberg atoms, *Physical Review A* 94, 062307 (2016).
- [67] D. Petrosyan, F. Motzoi, M. Saffman, and K. Mølmer, High-fidelity rydberg quantum gate via a two-atom dark state, *Physical Review A* 96, 042306 (2017).
- [68] X.-R. Huang, Z.-X. Ding, C.-S. Hu, L.-T. Shen, W. Li, H. Wu, and S.-B. Zheng, Robust rydberg gate via landau-zener control of förster resonance, *Physical Review A* 98, 052324 (2018).
- [69] I. I. Beterov, G. N. Hamzina, E. A. Yakshina, D. B. Tretyakov, V. M. Entin, and I. I. Ryabtsev, Adiabatic passage of radio-frequency-assisted förster resonances in rydberg atoms for two-qubit gates and the generation of bell states, *Physical Review A* 97, 032701 (2018).
- [70] M. Saffman, I. I. Beterov, A. Dalal, E. J. Pérez, and B. C. Sanders, Symmetric rydberg controlled-z gates with adiabatic pulses, *Physical Review A* 101, 062309 (2020).
- [71] A. Mitra, M. J. Martin, G. W. Biedermann, A. M. Marino, P. M. Poggi, and I. H. Deutsch, Robust mølmer-sørensen gate for neutral atoms using rapid adiabatic rydberg dressing, *Physical Review A* 101, 030301 (2020).
- [72] N. R. Hutzler, L. R. Liu, Y. Yu, and K.-K. Ni, Eliminating light shifts for single atom trapping, *New Journal of Physics* 19, 023007 (2017).
- [73] A. Cesa and J. Martin, Two-qubit entangling gates between distant atomic qubits in a lattice, *Physical Review A* 95, 052330 (2017).
- [74] X.-F. Shi and Y. Lu, Quantum gates with weak van der waals interactions of neutral rydberg atoms, *Physical Review A* 104, 012615 (2021).
- [75] A. M. Kaufman and K.-K. Ni, Quantum science with optical tweezer arrays of ultracold atoms and molecules, *Nature Physics* 17, 1324 (2021).
- [76] M. Marcuzzi, J. c. v. Minář, D. Barredo, S. de Léséleuc, H. Labuhn, T. Lahaye, A. Browaeys, E. Levi, and I. Lesanovsky, Facilitation dynamics and localization phenomena in rydberg lattice gases with position disorder, *Physical Review Letters* 118, 063606 (2017).
- [77] L. Béguin, A. Vernier, R. Chicireanu, T. Lahaye, and A. Browaeys, Direct measurement of the van der waals interaction between two rydberg atoms, *Physical Review Letters* 110, 263201 (2013).
- [78] Y. Yu, N. R. Hutzler, J. T. Zhang, L. R. Liu, J. D. Hood, T. Rosenband, and K.-K. Ni, Motional-ground-state cooling outside the lamb-dicke regime, *Physical Review A* 97, 063423 (2018).
- [79] X.-Q. Shao, T.-Y. Zheng, C. Oh, and S. Zhang, One-step achievement of robust multipartite greenberger-horne-zeilinger state and controlled-phase gate via rydberg interaction, *JOSA B* 31, 827 (2014).
- [80] S.-L. Su and W. Li, Dipole-dipole-interaction-driven antiblockade of two rydberg atoms, *Physical Review A* 104, 033716 (2021).
- [81] T. M. Graham, M. Kwon, B. Grinkemeyer, Z. Marra, X. Jiang, M. T. Lichtman, Y. Sun, M. Ebert, and M. Saffman, Rydberg-mediated entanglement in a two-dimensional neutral atom qubit array, *Physical Review Letters* 123, 230501 (2019).
- [82] X. Zhang, A. Gill, L. Isenhower, T. Walker, and M. Saffman, Fidelity of a rydberg-blockade quantum gate from simulated quantum process tomography, *Physical*

- Review A* 85, 042310 (2012).
- [83] G. Di Domenico, S. Schilt, and P. Thomann, Simple approach to the relation between laser frequency noise and laser line shape, *Applied optics* 49, 4801 (2010).
- [84] H. Levine, A. Keesling, A. Omran, H. Bernien, S. Schwartz, A. S. Zibrov, M. Endres, M. Greiner, V. Vuletić, and M. D. Lukin, High-fidelity control and entanglement of rydberg-atom qubits, *Physical Review Letters* 121, 123603 (2018).
- [85] I. S. Madjarov, J. P. Covey, A. L. Shaw, J. Choi, A. Kale, A. Cooper, H. Pichler, V. Schkolnik, J. R. Williams, and M. Endres, High-fidelity entanglement and detection of alkaline-earth rydberg atoms, *Nature Physics* 16, 857 (2020).
- [86] Y. Liu, Y. Sun, Z. Fu, P. Xu, X. Wang, X. He, J. Wang, and M. Zhan, Infidelity induced by ground-rydberg decoherence of the control qubit in a two-qubit rydberg-blockade gate, *Physical Review Applied* 15, 054020 (2021).
- [87] T. A. Johnson, E. Urban, T. Henage, L. Isenhower, D. D. Yavuz, T. G. Walker, and M. Saffman, Rabi oscillations between ground and rydberg states with dipole-dipole atomic interactions, *Physical Review Letters* 100, 113003 (2008).
- [88] D. Jaksch, J. I. Cirac, P. Zoller, S. L. Rolston, R. Côté, and M. D. Lukin, Fast quantum gates for neutral atoms, *Physical Review Letters* 85, 2208 (2000).
- [89] M. D. Lukin, M. Fleischhauer, R. Cote, L. M. Duan, D. Jaksch, J. I. Cirac, and P. Zoller, Dipole blockade and quantum information processing in mesoscopic atomic ensembles, *Physical Review Letters* 87, 037901 (2001).
- [90] E. Urban, T. A. Johnson, T. Henage, L. Isenhower, D. Yavuz, T. Walker, and M. Saffman, Observation of rydberg blockade between two atoms, *Nature Physics* 5, 110 (2009).
- [91] A. Gaëtan, Y. Miroshnychenko, T. Wilk, A. Chotia, M. Viteau, D. Comparat, P. Pillet, A. Browaeys, and P. Grangier, Observation of collective excitation of two individual atoms in the rydberg blockade regime, *Nature Physics* 5, 115 (2009).
- [92] Y. Zeng, P. Xu, X. He, Y. Liu, M. Liu, J. Wang, D. J. Papoular, G. V. Shlyapnikov, and M. Zhan, Entangling two individual atoms of different isotopes via rydberg blockade, *Physical Review Letters* 119, 160502 (2017).
- [93] S.-L. Su, Y. Gao, E. Liang, S. Zhang *et al.*, Fast rydberg antiblockade regime and its applications in quantum logic gates, *Physical Review A* 95, 022319 (2017).
- [94] S. Jandura and G. Pupillo, Time-Optimal Two- and Three-Qubit Gates for Rydberg Atoms, *Quantum* 6, 712 (2022).
- [95] C. Tuchendler, A. M. Lance, A. Browaeys, Y. R. P. Sortais, and P. Grangier, Energy distribution and cooling of a single atom in an optical tweezer, *Physical Review A* 78, 033425, (2008).
- [96] D. Yu, H. Wang, J.-M. Liu, S.-L. Su, J. Qian, and W. Zhang, Multiqubit toffoli gates and optimal geometry with rydberg atoms, *Physical Review Applied* 18, 034072 (2022).
- [97] S. Jandura, J. D. Thompson, and G. Pupillo, Optimizing rydberg gates for logical-qubit performance, *PRX Quantum* 4, 020336 (2023).
- [98] O. Gamel and D. F. V. James, Time-averaged quantum dynamics and the validity of the effective hamiltonian model, *Physical Review A* 82, 052106 (2010).
- [99] P. Doria, T. Calarco, and S. Montangero, Optimal control technique for many-body quantum dynamics, *Physical Review Letters* 106, 190501 (2011).